RSC Advances

PAPER

View Article Online
View Journal | View Issue

Cite this: *RSC Adv.*, 2017, **7**, 16295

Selective and sensitive colorimetric determination of cobalt ions using Ag–Au bimetallic nanoparticles

Dong Xu,[a] Hong Chen,[a] Qinlu Lin,*[a] Ziwei Li,[a] Tao Yang[a] and Zhiqin Yuan*[b]

Plasmonic nanoparticle-based colorimetric sensing has gained wide attention due to its advantages including rapidity, simplicity and expensive instrument-free characters. In the present study, Ag–Au bimetallic nanoparticles were proposed as novel optical probes to determine cobalt ion (Co^{2+}) concentration. The sensing mechanism is based on the fact that Co^{2+} can react with ethylenediamine (en) and $S_2O_3^{2-}$ to form $(en)_2CoS_2O_3^+$ on the nanoparticle surface, which can decrease the negative charge of the nanoparticle, reduce the repulsion between adjacent nanoparticles, and subsequently induce nanoparticle aggregation, was verified by dynamic light scattering. The effects of several parameters on the detection sensitivity, including the concentration of $S_2O_3^{2-}$ and en, pH value and incubation time, were investigated. The assay demonstrated high selectivity toward Co^{2+} in the presence of K^+, Cu^{2+}, Pb^{2+}, Ag^+, Zn^{2+}, Ba^{2+}, Mn^{2+}, Fe^{2+}, Fe^{3+}, Ni^{2+} and Hg^{2+}. Under optimal conditions, the absorbance ratio of A_{600}/A_{434} showed a linear relationship *versus* Co^{2+} concentration from 0 to 0.6 μM with a correlation coefficient (R^2) of 0.980, and the detection limit was calculated to be 0.02 μM. The practical application of the proposed nanoprobes was evaluated with river and tap water samples.

Received 21st January 2017
Accepted 7th March 2017

DOI: 10.1039/c7ra00900c

rsc.li/rsc-advances

1. Introduction

Plasmonic nanoparticle-based colorimetric methods for detecting analytes have gained growing interest because of their simplicity, low cost, rapid response and expensive instrument-free characters.[1–4] Various analytes including metal ions,[5,6] proteins,[7] DNA,[8,9] glucose,[10] H_2S[11] could be determined through elaborately designed strategies with high sensitivity and selectivity. Monometallic nanoparticles, in particular gold nanoparticles and silver nanoparticles, are the two most selected materials for developing colorimetric assays due to their prominent characteristics. Both gold and silver nanoparticles possess high absorption and scattering coefficients, high optical stability without photobleaching and photoblinking.[12,13] Gold nanoparticle is inert to oxidation, having stronger chemical stability and better biocompatibility. However, silver nanoparticles have the highest efficiency of absorption and scattering light compared to gold and copper materials. For example, the molar extinction coefficient of silver nanoparticles is 20-fold larger than that of gold nanoparticles in the same volume,[14] and the molar extinction coefficient is closely related to sensor sensitivity. Recently, Ag–Au bimetallic nanoparticles (BNPs, *e.g.*, Ag core–Au shell nanoparticles) have attracted increasing attentions because their specific optical and physical features, such as good catalytic capacity, surface-enhanced Raman scattering property.[15] They also can integrate the merits of the Ag and Au materials, that is, high plasmonic property of Ag and the stability of Au.[16] The bands of localized surface plasmonic resonance in the range of 400–550 nm can be conveniently tuned by varying their components while keeping the nanoparticle diameter constant.[17] Correspondingly, the BNP solution color could also vary from yellow to brown, to red by changing the components. Thus, BNP-based probes can provide low detection background, well stability and high sensitivity in assays. Despite of wide applications of Ag–Au BNPs, the studies on using Ag–Au BNPs as a platform in colorimetric sensors are still very rare.

Cobalt (Co^{2+}) is normally recognized as an essential element for human body, which acts as the metallic component of vitamin B12 and some metal loprotease. However, exposure to its excess amount can lead to serious health diseases.[18–20] For example, excess Co^{2+} could change the enzyme activities, cause oxidative stress and DNA damage.[21,22] It can also bring about low blood pressure, paralysis and even tissue carcinogenesis.[23] On the other side, the widespread applications of cobalt in industries and medical science increase its exposure risks. For example, cobalt is important for processing alloys with corrosion and heat resistance, strong magnetism and high-strength.[18] Cobalt is widely utilized in pigments in the glass and ceramics,[24] and lithium ion batteries.[25] In clinic, hip replacements are usually made from cobalt,[26,27] inevitably lifting serum cobalt levels of patients. Therefore, developing assays for detecting Co^{2+} is urgent. Up to now, atom absorption

[a]*National Engineering Laboratory for Rice and By-products Further Processing, Central South University of Forestry & Technology, Changsha 410004, China. E-mail: LinQL0403@163.com; Tel: +86-731-8562-3240*

[b]*State Key Laboratory of Chemical Resource Engineering, Beijing University of Chemical Technology, Beijing 100029, China. E-mail: yuanzq@mail.buct.edu.cn; Tel: +86-10-64411957*

spectroscopy,[28] fluorescent techniques[29] and electrochemical methods[30] were exploited for Co^{2+} determination. However, there are several shortcomings including time-consuming and complex sample preparation when using these techniques. In contrast, colorimetric methods with rapid response and simple preparation characters may benefit the development of Co^{2+} determination strategy.[31,32] Thereby, colorimetric method based on plasmonic nanoparticle may be an alternate owing to its specific virtues. Zhang *et al.* reported a colorimetric method for Co^{2+} quantification with a detection limit of 3.0×10^{-7} M based on Co^{2+} induces aggregation of thioglycolic acid capped gold nanoparticles.[33] In Sung's work, glutathione functionalized silver nanoparticles with the shapes of sphere, plate and rod as probes for Co^{2+} were investigated and it was found rod-type silver nanoparticles showed better selectivity.[34] Yao *et al.* synthesized triazole-carboxyl bifunctionalized silver nanoparticles by a click reaction to detect Co^{2+} sensitively.[35] Zhang *et al.* developed a label free colorimetric method for cobalt determination.[36] Annadhasan *et al.* reported a green method to fabricate gold nanoparticles under sunlight irradiation by using *N*-cholyl-L-valine as the reducing and capping agent, which demonstrated high selectivity and sensitivity toward Co^{2+}.[37] Nevertheless, the development of new colorimetric methods for Co^{2+} sensing is still appealing.

Herein, we developed a label-free method for sensing Co^{2+} in aqueous solutions by using Ag–Au BNPs fabricated by one-pot synthesis. The sensing is due to Co^{2+} can trigger the formation of $(en)_2CoS_2O_3^+$ in the presence of thiosulfate ($S_2O_3^{2-}$) and ethylenediamine (en), which decreases the repulsion between adjacent nanoparticles and causes the aggregation. This proposed method exhibited high selectivity toward Co^{2+} over other metal ions because of the involvement of a series of specific chemical reactions. The practical application of this method was further validated by detecting Co^{2+} in tap and river water samples.

2. Experimental

2.1 Chemicals

Hydrogen tetrachloroaurate(III) trihydrate ($HAuCl_4 \cdot 3H_2O$), silver nitrate ($AgNO_3$), polyvinyl pyrrolidone (PVP, 25k MW), trisodium citrate ($C_6H_5O_7Na_3 \cdot 2H_2O$), ethylenediamine (en), sodium thiosulfate ($Na_2S_2O_3$) and glycine were purchased from Sinopharm Chemical Reagent (China). Analytical grade chemicals including $CoSO_4 \cdot 7H_2O$, KCl, $CuSO_4 \cdot 5H_2O$, $Pb(NO_3)_2$, $ZnCl_2$, $BaCl_2$, $MnSO_4 \cdot H_2O$, $FeSO_4 \cdot 7H_2O$, $FeCl_3$, $NiCl_2 \cdot 6H_2O$, and $Hg(NO_3)_2$ were obtained from Sigma Aldrich. Deionized water (18.2 MΩ cm) was obtained from a Millipore system (Billerica, USA). All glassware was cleaned with fresh aqua regia ($HCl : HNO_3 = 3 : 1$) before use. Glycine–NaOH buffer solutions (0.1 M) with pH values ranging from 8.6 to 9.6 were prepared by glycine and NaOH and the pH values were measured with a benchtop Orion™ plus pH meter (Thermo-Fisher, USA).

2.2 Characterization

The UV-vis absorption spectra of the nanoparticles were obtained with a UV-1800 spectrophotometer (Shimadzu, Japan). Transmission electron microscopy (TEM) images of nanoparticles were collected with a JEOL JEM-1230 transmission electron microscope under operation of 100 kV (Hitachi, Japan). Photographs of nanoparticle solution was obtained with iphone 5. Dynamic light scattering (DLS) and zeta potential measurements were performed with a Zetasizer Nano ZS analyzer (Malvern, U.K.). X-ray photoelectron spectroscopy (XPS) was obtained on K-alpha 1063 X-ray photoelectron spectrometer (Thermo Fisher Scientific, USA) with Al Kα radiation operated at 72 W (6 mA emission current, 12 kV) and a base pressure of 10^{-9} mbar. Elemental mapping analysis was performed in the STEM mode on a Tecnai G^2 F20 field emission TEM (FEI, USA).

2.3 One-pot synthesis of Ag–Au BNPs

Ag–Au BNPs were prepared according to the previous reported papers with slight modifications.[17] In brief, 182 μL 0.1 M $AgNO_3$ and 250 μL 24.28 mM (1% in weight) $HAuCl_4$ solutions was added into 95.5 mL distilled water in a flask. The mixture was heated to boil in oil bath under constant stirring at 250 rpm. During reflux, 2 mL 1 wt% trisodium citrate was rapidly injected into the solution. Reflux of the solution for another 1 h was to insure the formation of colloid. During this process, the color of the solution would turn to yellow from colorless. After cooling, the colloid suspension was stored at 4 °C in refrigerator prior to use.

2.4 Sensitivity and selectivity of Co^{2+} sensing

A high concentration stock solution of $CoSO_4$ (0.1 M) was prepared and used to prepare standard solutions through a serial dilution. For Co^{2+} detection, 1000 μL the as prepared Ag–Au BNP suspension was first mixed with 710 μL 0.1 M glycine–NaOH buffers in 2 mL tube to make the ultimate solution pH value at 9.0. Then, 55 μL distilled water, 20 μL 0.05 M $Na_2S_2O_3$ and 200 μL Co^{2+} solution with different concentrations were injected into the tube in sequence. Finally, after 2 min equilibration at room temperature, 15 μL 1% v/v en solution was added to each tube. The photos and UV-vis spectra of the solutions were recorded during the 20 min window. The following metal ions were used to evaluate the selectivity of the BNP sensing system: K^+, Cu^{2+}, Pb^{2+}, Ag^+, Zn^{2+}, Ba^{2+}, Mn^{2+}, Fe^{2+}, Fe^{3+}, Ni^{2+} and Hg^{2+}.

2.5 Real sample analysis

Water samples obtained from Xiang River and tap water in campus were firstly centrifuged (12 000 rpm, 30 min) and then filtered through a 0.2 μm membrane to remove large suspended particles. The Co^{2+} detection procedure is the same as sensitivity test. 1000 μL of the as prepared Ag–Au BNP suspension was mixed with 710 μL 0.1 M glycine–NaOH buffers, 55 μL distilled water, 20 μL 0.05 M $Na_2S_2O_3$ and 200 μL of the tested samples sequentially. Finally, after 2 min equilibration at room temperature, 15 μL 1% v/v en solution was added to each tube. The photos and UV-vis spectrum of the solutions were recorded after 20 min.

3. Results and discussions

3.1 Principle of Co^{2+} detection

We prepared Ag–Au BNPs by a one-pot synthetic procedure.[38,39] According to the literature,[17] the BNPs have Ag core–Au shell structures, which endows them high stability. The molar ratio of Ag : Au was finally set to be 3 : 1, since the compromise was made between the strong optical properties of nanoparticles relating to the detection signals and the well chemical stability associating with convenient storage. The obtained Ag–Au BNP was characterized by camera, UV-vis spectra, TEM and XPS, as displayed in Fig. 1. The color of as-prepared nanoparticle solution was yellow, whose UV-vis spectrum peak was located at 434 nm. In contrast, the UV-vis peak of gold nanoparticle (AuNP) and silver nanoparticle (AgNP) with the same diameter are at 532 nm and 393 nm according to the Mie simulations, respectively.[40] The statistical size distribution of 132 nanoparticles was displayed in Fig. 1C. TEM results showed that these nanoparticles are spherical and monodisperse with a size of 28.6 ± 4.1 nm. Distribution of Ag and Au elements in BNPs proved that the nanoparticles consist of a predominant Ag core and a Au rich shell, which is consistent with the reported structure.[17] As shown in Fig. 1E, the valence of both Ag and Au in BNP XPS was zero due to the overdose of the reducing agent. After 1.2 μM Co^{2+} was added, the color of the solution turned to pale green from yellow due to the obvious aggregation of Ag–Au BNPs with the presence of $S_2O_3^{2-}$ and en (Fig. 1A(a) and (b)). The absorbance below 500 nm decreased, while that above 500 nm increased. The color alternation in our assay is different from that of pure AuNPs or AgNPs systems, in which AuNP solution would become purple or blue from red[2,3] and AgNP solution turns pale red from yellow.[2,41] We found that the value of A_{600}/A_{434} could effectively reflect the ratio of the dispersed to the aggregated Ag–Au BNPs, and thus was finally used to evaluate Co^{2+} in our study.

In order to further study the mechanism, we measured the hydraulic diameter and zeta potential of Ag–Au BNPs under different solution conditions, as shown in Fig. 2. As expected, an obvious increase on hydraulic diameter of Ag–Au BNP (from 50.7 nm to 190.1 nm) was observed, indicating the color change of solution can be assigned to the aggregation of Ag–Au BNPs. With the addition of chemicals, the surface potential of Ag–Au BNPs also changed. When $S_2O_3^{2-}$ was mixed with Ag–Au BNP solution, $S_2O_3^{2-}$ was immediately and strongly absorbed onto nanoparticle surface due to the strong affinity between sulfur and gold.[42] The zeta potential of Ag–Au BNP changed to

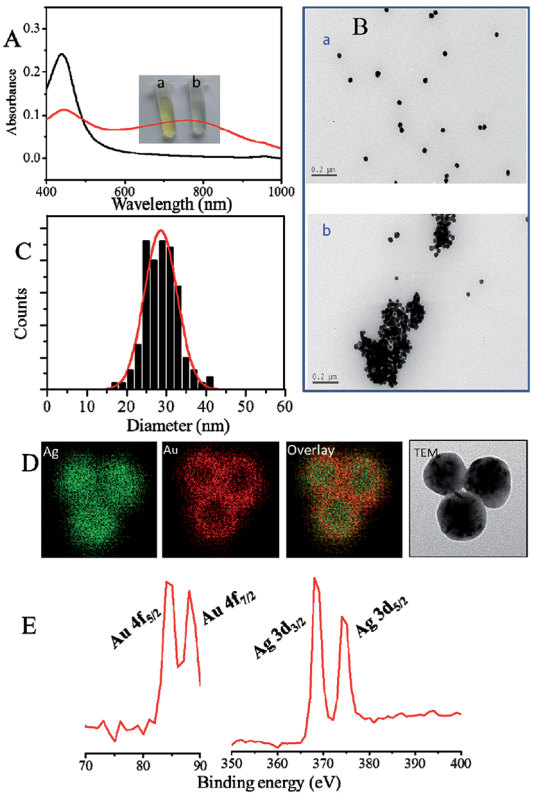

Fig. 1 UV-vis spectra (A) and TEM images (B) of Ag–Au BNPs in 0.1 M glycine–NaOH buffer solution (pH = 9.0) containing 0.5 mM $S_2O_3^{2-}$ and en (0.0075%, v/v) in the absence (a) and presence (b) of 1.2 μM Co^{2+}. (C) The statistic diameter distribution of the Ag–Au BNPs. (D) Elemental analysis of Ag–Au BNPs (from left to right): the mapping image of Ag and Au, the overlay image and the corresponding TEM image. The size of each image is 100 × 100 nm. (E) XPS spectra of Au 4f (left) and Ag 3d (right) for Ag–Au BNPs.

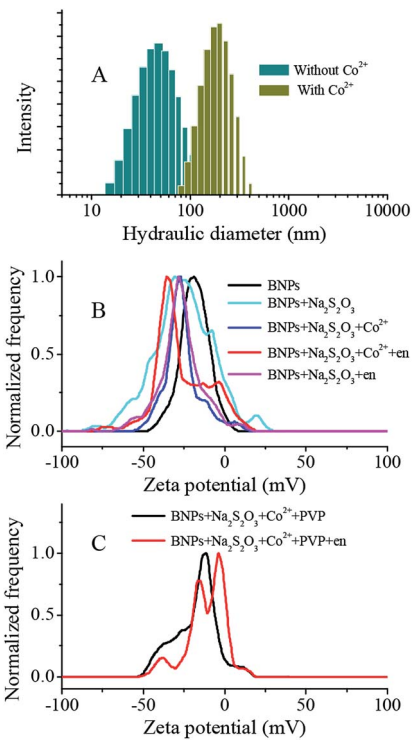

Fig. 2 (A) Hydrodynamic size distribution of Ag–Au BNPs without and with the addition of 0.8 μM Co^{2+} in the presence of 0.5 mM $Na_2S_2O_3$, 0.0075% (v/v) en at pH 9.0. (B) Zeta potential of Ag–Au BNPs without and with the addition of 0.5 mM $Na_2S_2O_3$, 0.5 mM $Na_2S_2O_3$/0.8 μM Co^{2+}, 0.5 mM $Na_2S_2O_3$/0.8 μM Co^{2+}/0.0075% en and 0.5 mM $Na_2S_2O_3$/0.0075% en, respectively. (C) Zeta potential of Ag–Au BNPs upon adding 0.02% PVP, 0.5 mM $Na_2S_2O_3$ and 0.8 μM Co^{2+} at pH 9.0 in the absence and presence of 0.0075% en.

−26.9 mV from −18 mV. $S_2O_3^{2-}$ coated Ag–Au BNPs are very stable due to the strong electrostatic repulsions between negatively charged nanoparticles even at high ionic strength. These nanoparticles do not aggregate with the presence of 0.0075% en and their zeta potential (−26.1 mV) was unchanged, partially because en does not react with $S_2O_3^{2-}$ directly. Upon the addition of Co^{2+}, Co^{2+} could quickly react with en to form $Co(en)_3^{2+}$ first and then $Co(en)_3^{2+}$ was readily oxidized to $Co(en)_3^{3+}$ by the dissolved oxygen in water.[43] Afterwards, $Co(en)_3^{3+}$ would attack $S_2O_3^{2-}$ on nanoparticle surface to form positively-charged $(en)_2CoS_2O_3^{+}$.[44] As a result, the formed $(en)_2CoS_2O_3^{+}$ decreased the negative charge of nanoparticle and triggered the aggregation of nanoparticle. However, the measured zeta potential become more negative (−31.6 mV) after the formation of aggregates, which can not conclude the surface charge of single nanoparticles was reduced. To bypass the problem, 0.02 wt% PVP, a polymer that is widely applied to stabilize the nanoparticle, was added to the solution to prevent nanoparticle aggregation after adding Co^{2+}. PVP stabilized nanoparticles have a potential of −13.8 mV, but after the addition of Co^{2+}, an increased potential around −4.0 mV emerged (Fig. 2C). This result confirmed that Co^{2+} indeed reduced the negative charge and caused the aggregation of Ag–Au BNPs. Scheme 1 depicted the mechanism of Co^{2+} detection.

3.2 Establishment of the colorimetric sensing method for Co^{2+}

As mentioned above, the Co^{2+} induced nanoparticle aggregation was attributed to the formation of $(en)_2CoS_2O_3^{+}$ at the surface of Ag–Au nanoparticles. Since this reaction needs the participation of several reagents, a systematic investigation was performed to optimize these parameters by monitoring the ratio of absorbance ratio $(A_{600}/A_{434})_{sample}/(A_{600}/A_{434})_{blank}$ changes at 600 and 434 nm, including the concentration of $S_2O_3^{2-}$ and en, solution pH value and the incubation time. During this study, the concentration of Co^{2+} of 1 μM was fixed.

The content of $S_2O_3^{2-}$ in the range of 0–1.0 mM was investigated when en was fixed at 0.0075% and the pH value at 9.2 in the presence (sample) and absence (blank) of Co^{2+}, as illustrated in Fig. 3. With the increasing $S_2O_3^{2-}$ concentration, $(A_{600}/A_{434})_{blank}$ remained unchanged, but the values of $(A_{600}/A_{434})_{sample}$ and $(A_{600}/A_{434})_{sample}/(A_{600}/A_{434})_{bank}$ increased gradually and reached to the top above 0.5 mM. The possible explanation is that, at low $S_2O_3^{2-}$ concentration, the surface of nanoparticle was not completely coated by $S_2O_3^{2-}$ and thus there was no enough sites on nanoparticle for $Co(en)_3^{3+}$ combination. While at high $S_2O_3^{2-}$ concentration (>0.5 mM), the surface of nanoparticle is totally occupied and free $S_2O_3^{2-}$ exists in solution. We suppose $Co(en)_3^{3+}$ tends to react with $S_2O_3^{2-}$ at particle surface probably due to the strong electrostatic attraction between $Co(en)_3^{3+}$ and the high negatively charged surface. Consequently, 0.5 mM $S_2O_3^{2-}$ was chosen for the assay.

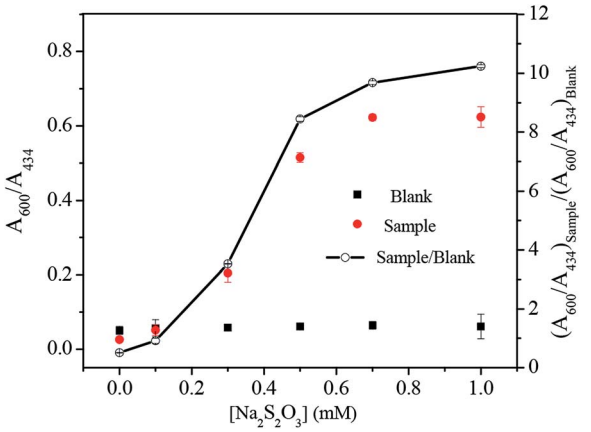

Fig. 3 Absorbance ratio $(A_{600}/A_{434})_{blank}$, $(A_{600}/A_{434})_{sample}$ and $(A_{600}/A_{434})_{sample}/(A_{600}/A_{434})_{blank}$ of Ag–Au BNPs solution *versus* the concentration of $Na_2S_2O_3$. Experimental conditions: 1.0 μM Co^{2+}, pH = 9.2, 0.0075% (v/v) en, 20 min incubation time.

It is well-known that solution pH could influence the interactions of nanoparticle with capping molecules, and thus alter nanoparticle stability, sensitivity and selectivity of the assay. We investigated the effect of solution pH in the range of 8.6–9.6. As shown in Fig. 4, $(A_{600}/A_{434})_{sample}/(A_{600}/A_{434})_{blank}$ reached the maximum value at pH 9.0. It is possible because low pH could cause decomposition of $S_2O_3^{2-}$, since its stability is proportional to pH. On the other hand, protonated en can hinder the

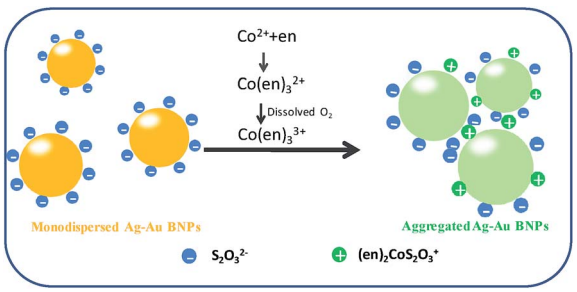

Scheme 1 Schematic illustration of colorimetric Co^{2+} detection using Ag–Au BNPs.

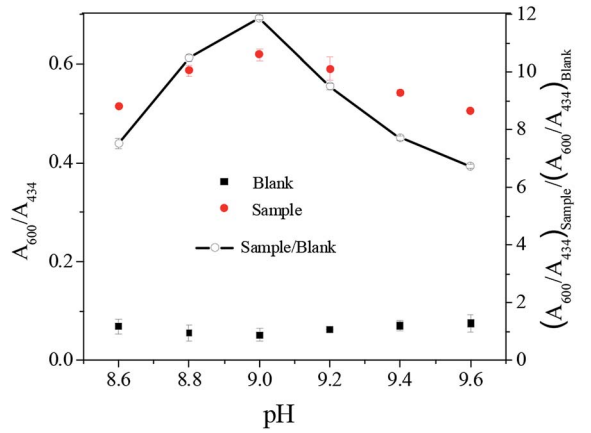

Fig. 4 Absorbance ratio $(A_{600}/A_{434})_{blank}$, $(A_{600}/A_{434})_{sample}$ and $(A_{600}/A_{434})_{sample}/(A_{600}/A_{434})_{blank}$ of Ag–Au BNPs solution *versus* solution pH. Experimental conditions: 1.0 μM Co^{2+}, 0.5 mM $S_2O_3^{2-}$, 0.0075% (v/v) en, incubation time 20 min.

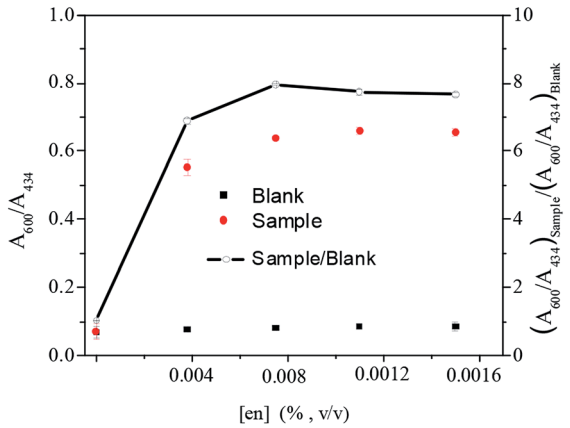

Fig. 5 Absorbance ratios $(A_{600}/A_{434})_{blank}$, $(A_{600}/A_{434})_{sample}$ and $(A_{600}/A_{434})_{sample}/(A_{600}/A_{434})_{blank}$ of Ag–Au BNPs solution *versus* en concentration. Experimental conditions: 1.0 μM Co^{2+}, 0.5 mM $S_2O_3^{2-}$, pH = 9.0, incubation time 20 min.

formation of $(en)_2CoS_2O_3^+$. Conversely, extremely high pH may decrease the stability of nanoparticles *via* decreasing the surface repulsion and reduce oxidizing capacity of dissolved O_2 on Co^{2+}. Therefore, pH 9.0 was finally opted for the assay. Similarly, as demonstrated in Fig. 5, the optimal en concentration was determined to be 0.0075% (v/v).

The incubation time is a key point for the colorimetric assays. The relationship between the ratio of A_{600}/A_{434} and incubation time was obtained by recording the UV-vis spectra of Ag–Au nanoparticle solution after the addition of 1 μM Co^{2+}, as shown in Fig. 6. It can be seen that $(A_{600}/A_{434})_{sample}$ increased with the increasing incubation time, and reached a flatform after 20 min. The incubation time of 20 min in Co^{2+} assays was selected.

3.3 Co^{2+} sensing in aqueous media

Selectivity of sensing methods is very important for its practical applications. In this study, the ratio of A_{600}/A_{434} of Ag–Au nanoparticle solution upon addition of various metal ions including K^+, Cu^{2+}, Pb^{2+}, Ag^+, Zn^{2+}, Ba^{2+}, Mn^{2+}, Fe^{2+}, Fe^{3+}, Ni^{2+} and Hg^{2+} under optimal conditions were measured to investigate whether the aggregation induced by Co^{2+} is specific. As manifested in Fig. 7, none of these metal ions (K^+, Pb^{2+}, Ag^+, Zn^{2+}, Ba^{2+}, Mn^{2+}, Fe^{2+}, Fe^{3+}, Ni^{2+}, Hg^{2+}: 100 μM; Cu^{2+}: 5 μM) can induce comparable aggregation of Ag–Au nanoparticle as 1 μM Co^{2+} did. Such a high selectivity toward Co^{2+} of this method might be ascribed to the specific chemical reactions in Co^{2+}, en and $S_2O_3^{2-}$ system. First, Co^{2+} can react with en to generate chelating complex $Co(en)_3^{2+}$; second, the complex with low Gibbs free energy can be oxidized into $Co(en)_3^{3+}$ by dissolved oxygen; third, by reacting with $S_2O_3^{2-}$, $Co(en)_3^{3+}$ could effectively reduce the negative charge on gold surface and lead to nanoparticle assembly. Despite of the formation of other metal–en complex, the lacking valence conversion or low reactivity to $S_2O_3^{2-}$ lead to different results upon adding other metal ions. Thus, our system showed excellent selectivity toward Co^{2+}.

For the sensitivity evaluation, absorption spectra of Ag–Au nanoparticle solution were recorded after adding Co^{2+} with different concentrations (0, 0.05, 0.1, 0.2, 0.4, 0.6, 0.8, 1.0 and 1.2 μM). Upon increasing Co^{2+} concentration, the absorbance at 434 nm decreased, while that of new generated peaks in the range of 600–850 nm increased. The appearance of absorption shifted probably due to the occurrence of fusion between aggregated nanoparticles, which is confirmed by TEM results. The corresponding photographs of solution changed from yellow to light yellow, and finally pale green. As can be seen from Fig. 8, the ratio of A_{600}/A_{434} of Ag–Au nanoparticle solution increased gradually upon increasing Co^{2+} concentration, and a typical S-shaped curve is acquired. At 0.6 μM, the curve has nearly reached the plateau, which is lower than that tested by gold nanoparticle.[36] A linear relationship was obtained with Co^{2+} in the range from 0 to 0.6 μM and was easily described by the linear equation with a correlation coefficient (R^2) of 0.980: $y = 0.085 + 1.055x$, where y and x are the ratio of A_{600}/A_{434} and Co^{2+} concentration, respectively. The limit of detection toward Co^{2+} of our assay was calculated to be 0.02 μM (3σ), which is

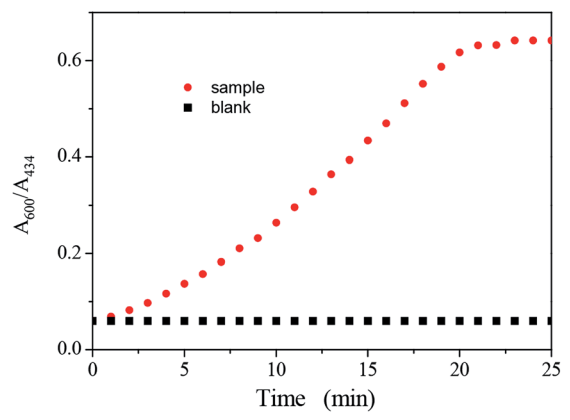

Fig. 6 Plots of the time-dependent absorbance ratio (A_{600}/A_{434}) of Ag–Au BNPs solution *versus* reaction time without (black) and with (red) the addition of 1.0 μM Co^{2+} in the presence of 0.5 mM $S_2O_3^{2-}$, 0.0075% (v/v) en at pH 9.0.

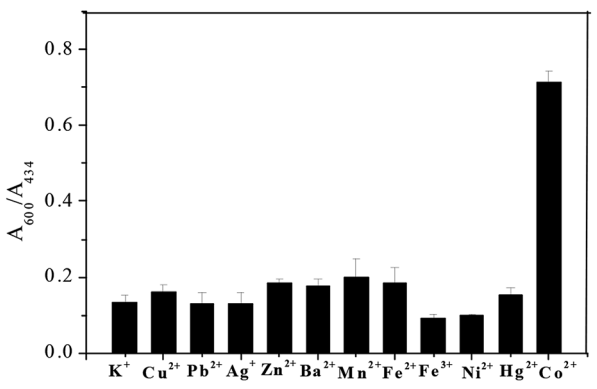

Fig. 7 The absorbance ratio (A_{600}/A_{434}) of Ag–Au BNPs solution upon the addition of various metal ions at pH 9.0 in the presence of 0.5 mM $S_2O_3^{2-}$ and 0.0075% (v/v) en. Concentrations: 100 μM K^+, Pb^{2+}, Ag^+, Zn^{2+}, Ba^{2+}, Mn^{2+}, Fe^{2+}, Fe^{3+}, Ni^{2+}, Hg^{2+}, 5 μM Cu^{2+} and 1 μM Co^{2+}.

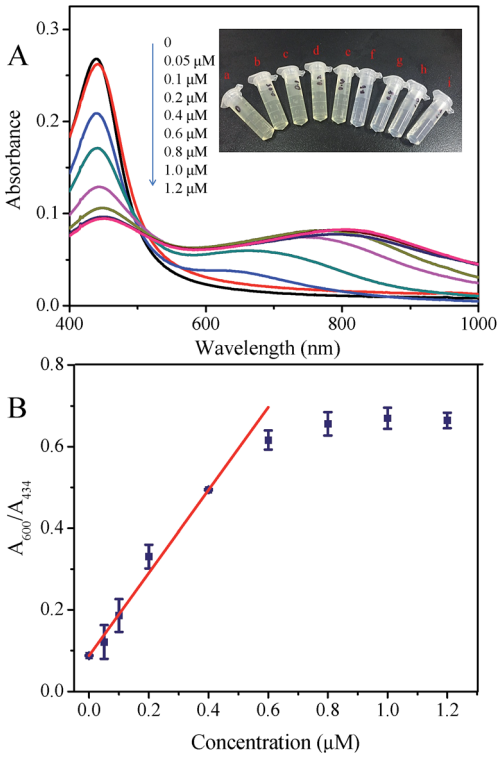

Fig. 8 (A) Absorption spectra and solution color of Ag–Au BNPs solution with the addition of various concentrations of Co^{2+} (from (a to i): 0, 0.05, 0.1, 0.2, 0.4, 0.6, 0.8, 1.0 and 1.2 μM). (B) Corresponding plots of absorbance ratio (A_{600}/A_{434}) *versus* the concentration of Co^{2+}.

lower than those reported colorimetric methods.[33–36] Taken together, we could conclude that Ag–Au nanoparticle could be capable probes for Co^{2+} sensing.

3.4 Quantification of Co^{2+} in real samples

To investigate the potential application of the designed system in real samples, we tested tap and river water samples with spiked Co^{2+}. The water samples did not induce the color change of Ag–Au nanoparticle solution without extra Co^{2+}. The atomic absorption spectrum analysis demonstrated that the Co^{2+} content is below the detection limit of our method. Further, spike-recoveries tests showed that the recoveries for 0.4 μM Co^{2+} in tap water and 0.3 μM in river water were 102% and 106%, respectively. These results suggest the accuracy of the proposed method and its practicability for Co^{2+} detection in environmental samples.

4. Conclusions

In this study, a simple and selective colorimetric method of Co^{2+} detection based on the aggregation of Ag–Au BNPs was developed. These BNPs used in this methods guarantee the high chemical stability and optical signals. Based on the special reactions in Co^{2+}, en and $S_2O_3^{2-}$ system, this assay can achieve the Co^{2+} determination with the presence 100-fold other ions such as K^+, Pb^{2+}, Ag^+, Zn^{2+}, Ba^{2+}, Mn^{2+}, Fe^{2+}, Fe^{3+}, Ni^{2+} and Hg^{2+} and 5-fold Cu^{2+}. This method has a low LOD of 0.02 μM with a linear range in 0–0.6 μM. The rapid response within 20 min makes the assay capable of real-time and on-site Co^{2+} sensing applications. Our assay also showed effective applications in the real water sample analysis. New avenues for the design of bimetallic sensors for other analytes based on a similar strategy might be opened up in the analytical and related fields by preparing BNP with different sizes and compositions.

Acknowledgements

This work was supported by funding from the National Natural Science Foundation of China (21505162, 21605003, 31571874), the Grain-Oil Process and Quality Control 2011 Collaborative and Innovative Grant from Hunan province, the China Postdoctoral Science Foundation (2016M600899), and the Fundamental Research Funds for the Central Universities (BUCTRC201619, ZY1625).

References

1 S. Zeng, K.-T. Yong, I. Roy, X.-Q. Dinh, X. Yu and F. Luan, *Plasmonics*, 2011, **6**, 491–506.
2 D. Vilela, M. C. González and A. Escarpa, *Anal. Chim. Acta*, 2012, **751**, 24–43.
3 W. Zhao, M. A. Brook and Y. Li, *ChemBioChem*, 2008, **9**, 2363–2371.
4 Z. Yuan, C. C. Hu, H. T. Chang and C. Lu, *Analyst*, 2016, **141**, 1611–1626.
5 G. Sener, L. Uzun and A. Denizli, *Anal. Chem.*, 2013, **86**, 514–520.
6 Z. Weng, H. Wang, J. Vongsvivut, R. Li, A. M. Glushenkov, J. He, Y. Chen, C. J. Barrow and W. Yang, *Anal. Chim. Acta*, 2013, **803**, 128–134.
7 T.-S. Lai, T.-C. Chang and S.-C. Wang, *Sens. Actuators, B*, 2017, **239**, 9–16.
8 M. Mancuso, L. Jiang, E. Cesarman and D. Erickson, *Nanoscale*, 2013, **5**, 1678–1686.
9 L. Guo, Y. Xu, A. R. Ferhan, G. Chen and D.-H. Kim, *J. Am. Chem. Soc.*, 2013, **135**, 12338–12345.
10 Y. Jiang, H. Zhao, Y. Lin, N. Zhu, Y. Ma and L. Mao, *Angew. Chem., Int. Ed.*, 2010, **122**, 4910–4914.
11 Z. Yuan, F. Lu, M. Peng, C. W. Wang, Y. T. Tseng, Y. Du, N. Cai, C. W. Lien, H. T. Chang and Y. He, *Anal. Chem.*, 2015, **87**, 7267–7273.
12 S. Palomba, M. Danckwerts and L. Novotny, *J. Opt. A: Pure Appl. Opt.*, 2009, **11**, 733–736.
13 A. M. Schrand, L. K. Braydichstolle, J. J. Schlager, L. Dai and S. M. Hussain, *Nanotechnology*, 2008, **19**, 1694–1706.
14 J.-S. Lee, A. K. Lytton-Jean, S. J. Hurst and C. A. Mirkin, *Nano Lett.*, 2007, **7**, 2112–2115.
15 B. W. Boote, H. Byun and J. H. Kim, *J. Nanosci. Nanotechnol.*, 2014, **14**, 1563–1577.
16 S. W. Verbruggen, M. Keulemans, J. A. Martens and S. Lenaerts, *J. Phys. Chem. C*, 2013, **117**, 19142–19145.
17 M. A. Uppal, M. B. Ewing and I. P. Parkin, *Eur. J. Inorg. Chem.*, 2011, **2011**, 4534–4544.

18 R. Lauwerys and D. Lison, *Sci. Total Environ.*, 1994, **150**, 1–6.
19 S. Mahey, R. Kumar, R. Arora, J. Mahajan, S. Arora, R. Bhardwaj and A. K. Thukral, *SpringerPlus*, 2016, **5**, 930.
20 P. J. Santander, Y. Kajiwara, H. J. Williams and A. I. Scott, *Bioorg. Med. Chem.*, 2006, **14**, 724–731.
21 L. Begovic, S. Mlinaric, J. A. Dunic, Z. Katanic, Z. Loncaric, H. Lepedus and V. Cesar, *Aquat. Toxicol.*, 2016, **175**, 117–126.
22 K. Al-Habsi, E. H. Johnson, I. T. Kadim, A. Srikandakumar, K. Annamalai, R. Al-Busaidy and O. Mahgoub, *Vet. J.*, 2007, **173**, 131–137.
23 D. Galaris and A. Evangelou, *Crit. Rev. Oncol. Hematol.*, 2002, **42**, 93–103.
24 M. Gaudon, L. Robertson, E. Lataste, M. Duttine, M. Ménétrier and A. Demourgues, *Ceram. Int.*, 2014, **40**, 5201–5207.
25 A. K. Mondal, H. Liu, Z.-F. Li and G. Wang, *Electrochim. Acta*, 2016, **190**, 346–353.
26 X. Mao, A. A. Wong and R. W. Crawford, *Med. J. Aust.*, 2011, **194**, 649–651.
27 D. L. Back, D. A. Young and A. J. Shimmin, *Clin. Orthop. Relat. Res.*, 2005, **438**, 177–181.
28 S. Cadore, R. D. Goi and N. Baccan, *J. Braz. Chem. Soc.*, 2005, **16**, 957–962.
29 S. H. Mashraqui, M. Chandiramani, R. Betkar and K. Poonia, *Tetrahedron Lett.*, 2010, **51**, 1306–1308.
30 I. M. Isa, S. N. A. Dahlan, N. Hashim, M. Ahmad and S. A. Ghani, *Int. J. Electrochem. Sci.*, 2012, **7**, 7797–7808.
31 Y. Li, J. Wu, X. Jin, J. Wang, S. Han, W. Wu, J. Xu, W. Liu, X. Yao and Y. Tang, *Dalton Trans.*, 2014, **43**, 1881–1887.
32 J. R. Zhou, D. P. Liu, Y. He, X. J. Kong, Z. M. Zhang, Y. P. Ren, L. S. Long, R. B. Huang and L. S. Zheng, *Dalton Trans.*, 2014, **43**, 11579–11586.
33 F. Zhang, L. Zeng, Y. Zhang, H. Wang and A. Wu, *Nanoscale*, 2011, **3**, 2150–2154.
34 H. K. Sung, S. Y. Oh, C. Park and Y. Kim, *Langmuir*, 2013, **29**, 8978–8982.
35 Y. Yao, D. Tian and H. Li, *ACS Appl. Mater. Interfaces*, 2010, **2**, 684–690.
36 Z. Zhang, J. Zhang, T. Lou, D. Pan, L. Chen, C. Qu and Z. Chen, *Analyst*, 2011, **137**, 400–405.
37 M. Annadhasan, J. Kasthuri and N. Rajendiran, *RSC Adv.*, 2015, **5**, 11458–11468.
38 B. Rodríguez-González, A. Burrows, M. Watanabe, C. J. Kiely and L. M. L. Marzán, *J. Mater. Chem.*, 2005, **15**, 1755–1759.
39 J. Yang, J. Y. Lee and H.-P. Too, *J. Phys. Chem. B*, 2005, **109**, 19208–19212.
40 C. F. Bohren and D. R. Huffman, in *Absorption and Scattering of Light by Small Particles*, Wiley, 1998.
41 H. Wei, C. Chen, B. Han and E. Wang, *Anal. Chem.*, 2008, **80**, 7051–7055.
42 Y. Y. Chen, H. T. Chang, S. Yenchun, H. Yulun, C. Chengkang and C. C. Huang, *Anal. Chem.*, 2009, **81**, 9433–9439.
43 J. Work and J. P. McReynolds, *Inorg. Synth.*, 1946, **2**, 221–222.
44 A. Murdock, T. Tyree, W. Otterbein, L. Kinney, M. Carreras, J. N. Cooper and R. Elder, *Inorg. Chem.*, 1985, **24**, 3674–3679.